Upscaling hydraulic conductivity by means of entropy of terrain curvature representation

Marcello Niedda

Dipartimento di Ingegneria del Territorio, Universita di Sassari, Sassari, Italy

Received 2 October 2003; revised 13 February 2004; accepted 24 February 2004; published 15 April 2004.

[1] The effects of topography resolution on upscaling point-scale processes and parameters on watershed hydrology numerical routing are investigated. Parsimonious continuous simulation was applied to two forested catchments with shallow and sloping soils, one medium-sized (123 km^2) and one small-sized (4.5 km^2), where saturation excess runoff prevails. The computed discharge showed highest sensitivity to spatial resolution, due to smoothing effects during aggregation of the digital elevation model caused by a coarse grid. The loss of information content of terrain curvature as consequence of the averaging procedure was related to the amplification factor required for the soil hydraulic conductivity to compensate the resulting retardation of the runoff hydrograph. A scaling relation has been developed that links soil hydraulic conductivity measured at the point-scale with that required at the typically much coarser modeling scale. The entropy concept for the measurement of information loss could be a good index for parameter rescaling of other basins where the terrain curvature is similarly scale-dependent. *INDEX TERMS:* 1860 Hydrology: Runoff and streamflow; 1829 Hydrology: Groundwater hydrology; 1824 Hydrology: Geomorphology (1625); 3230 Mathematical Geophysics: Numerical solutions; *KEYWORDS:* distributed modeling, entropy, finite difference schemes, grid DEM, information content, scale effect

Citation: Niedda, M. (2004), Upscaling hydraulic conductivity by means of entropy of terrain curvature representation, *Water Resour. Res.*, *40*, W04206, doi:10.1029/2003WR002721.

1. Introduction

[2] In recent decades the hydrological community has increasingly improved its understanding of the generation and routing mechanisms of surface and subsurface flow in river basins. The rapid development in computing capacity has played an important role in this improvement, and has allowed these mechanisms to be simulated by spatially distributed mathematical models [e.g., *Abbott et al.*, 1986; *Grayson et al.*, 1992a; *Beven et al.*, 1995; *Refsgaard*, 1997]. Practical applications of the distributed watershed simulation are becoming increasingly realistic through improvements in computer technology and field observations. Surface and subsurface flow dynamics can be simulated by solving the partial differential equations based on conservation of mass and momentum and through the use of finite difference (or finite element) numerical schemes. This kind of modeling requires numerical discretization of the time and space coordinates, and each time step is solved on a space-grid system. In this manner model variables and parameters are defined for each computational grid element and the spatial variation of the physical environment where the flow processes take place may be taken into account [*Jensen and Mantoglu*, 1992; *Singh and Woolhiser*, 2002].

[3] In distributed modeling the parameter values vary from grid element to grid element depending on the field measurements and numerical estimates. The high natural variability of the climate, topography, soil and vegetation in the space domain is one of the major problems in watershed modeling, as the scale of the available data is often too coarse when compared with the scale of the physical processes being represented [*Beven*, 1989; *Grayson et al.*, 1992b; *Rosso*, 1994; *Bloschl and Sivapalan*, 1995]. A traditional approach consists of using the minimum level of spatial scale which adequately represents the spatial heterogeneity of a watershed and in this way explicit representation of variability is not necessary [*Wood et al.*, 1988; *Moore and Grayson*, 1991; *Woods et al.*, 1995].

[4] A model of the hydrological processes at the basin-scale or larger, from a few km^2 to thousands of km^2, is needed in many practical applications, from hydrology and water resources management to atmospheric and environmental studies. The use of small-scale process descriptions at larger scales is the other major problem in watershed modeling. This is because the hydrologic conservation equations are derived at the point-scale within a differential control volume, they are tested in field plot or laboratory studies and their use on larger scales (the upscaling procedure) may require effective parameters that differ from those estimated from measurements. As stated by *Bathurst and O'Connel* [1992], it is useful to know whether model parameters need to be recalibrated for application at different grid scales and whether there is a grid scale above which the parameter calibrated values diverge significantly from the measured values. The use of the aggregation of spatial attributes as an approach to the scale problem is not considered generally adequate by *Beven* [1995]. *Bergstrom and Graham* [1998] state that "when shifting scales, a shift in parameter values might be necessary." This means that the model structure is generally applicable, but not the parameters. *Refsgaard et al.* [1999] state that "it is

0043-1397/04/2003WR002721$09.00

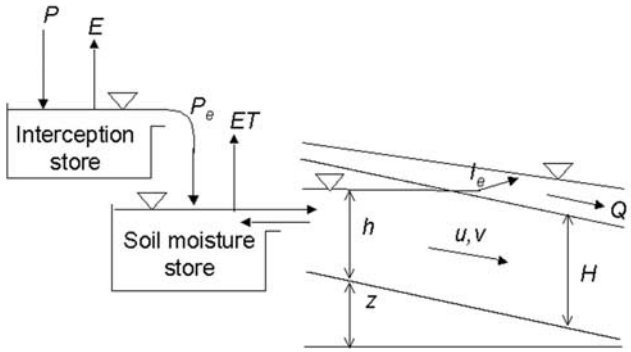

Figure 1. Conceptual representation for each space-grid cell of the vertical and lateral flows between soil, surface, and atmosphere domains.

generally not possible to apply the same model without recalibration at small and large scales." *Kavvas* [1999] states that "a fundamental problem is how to upscale the existing point-scale conservation equations to the increasingly larger spatial scales" but argues that these equations may still be quite parsimonious and need not be made more complicated.

[5] Although there has been extensive research on scale effects and grid resolution for atmospheric and hydrologic processes and geological heterogeneity over the past decade, no conclusive answer has been found. This is particularly true in watershed simulation [e.g., *Finnerty et al.*, 1997; *Winchell et al.*, 1998; *Koren et al.*, 1999; *Singh and Woolhiser*, 2002]. Some studies based on TOPMODEL showed how the model parameters were dependent on grid resolution [e.g., *Zhang and Montgomery*, 1994; *Bruneau et al.*, 1995; *Mendicino and Sole*, 1997; *Saulnier et al.*, 1997; *Valeo and Moin*, 2000; *Wolock and McCabe*, 2000]. Similar effects were found in other studies based on MIKE-SHE code applications [e.g., *Refsgaard*, 1997; *Refsgaard et al.*, 1999; *Vàzquez et al.*, 2002]. Many of these authors emphasize that a crucial point is the degree of discretization used to describe the 3-D nature of landscapes by means of a grid digital elevation model (DEM). They highlight how the model output is influenced by this. Topography is one of the main factors governing watershed dynamics, particularly in landscapes where lateral flows are dominant over vertical flows. However, important terrain details, such as the presence of incised streams, are not properly represented even when grid resolution is high. Thus many of the characteristics derived from DEMs are scale-dependent. The change of scale (grid size) in topographic discretization means that the flow process parameters must be recalibrated [*Grayson and Bloschl*, 2000].

[6] In recent years entropy theory has been applied in many areas in hydrology [*Singh*, 1997], and has also been used to measure the lack of information about a system (Shannon entropy). According to the informational entropy theory, if records are aggregated there is a reduction in information content. Some authors have investigated the scale problem and the effects of spatial aggregation of topographic data using the information content concept [*Vieux*, 1993; *Mendicino and Sole*, 1997; *Kuo et al.*, 1999]. They correlated the information loss to the errors in predicted runoff. The goal of this work is to relate the information content of terrain topographic representation to the accuracy of numerical schemes used to solve differential hydrologic conservation equations at the grid scale, and thus improve understanding of the grid resolution effects on the scale parameterization problem. To do this, a finite difference distributed model for the continuous simulation of the coupled subsurface channel flow [*Niedda*, 2000], was applied to two steep forested watersheds, one medium and one small sized. Along the lines of *Grayson et al.* [1992a] the modeling aims to minimize the number of parameters and processes represented while the flow routing components are physically based. Subsurface flow is simplified to a 2-D horizontal representation. Surface flow is simplified to a kinematic 1-D representation along the channel network. Since on shallow and sloping soils with high infiltration capacity the saturation excess mechanism of runoff production prevails [*Dunne and Black*, 1970; *Mosley*, 1979; *Pearce*, 1990], the infiltration excess mechanism is ignored. Topography is discretized by the grid DEM, which also defines the computational grid of the finite difference numerical schemes. Scale effects on hydrologic simulation are investigated using grid sizes of 5, 10, 25, 50, 100, and 250 m.

2. Governing Equations

[7] Surface interception and soil moisture store, evapotranspiration, 1D open channel flow and 2-D horizontal subsurface flow have been modeled in this study. Vertical and lateral flows between soil, surface and atmosphere domains are shown in the conceptual representation in Figure 1, where P is precipitation, E is evaporation from interception storage of capacity S, and ET is actual evapotranspiration. There is no infiltration equation and all excess precipitation P_e from interception storage enters the soil [*Moore and Grayson*, 1991; *Wigmosta et al.*, 1994]. Soil moisture θ varies between soil porosity ϕ and residual content, and for simplicity has been set at zero. It is assumed that soil thickness H first becomes wet up to the moisture content θ_{33} held at -33 kPa matric potential [*Rawls et al.*, 1993]. Only when the soil moisture exceeds θ_{33} do excess volumes constitute an input for the subsurface flow governed by Darcy's law. The zero-flow boundary condition is adopted at the catchment divide and at the base of the active permeable layer. Following *Anderson and Burt* [1977], the capillary fringe is not differentiated from the saturated zone. When the height of the water table h intercepts the ground surface ($h > H$), saturation excess I_e, is an input in surface flow. Surface runoff propagates downstream along the channel network and, if it reaches areas that are not yet saturated ($h < H$), downslope reinfiltration is allowed. The differential equations describing unsteady and spatially varied groundwater and open channel flow can be expressed as

$$n_e \frac{\partial h}{\partial t} + \frac{\partial (hu)}{\partial x} + \frac{\partial (hv)}{\partial y} = P_e - ET - I_e, \quad \text{with } \theta > \theta_{33}, \tag{1a}$$

$$I_e = 0 \qquad \text{if } 0 \le h \le H, \tag{1b}$$

$$I_e = \frac{n_e (h - H)}{dt} \quad \text{if } h > H; \tag{1c}$$

$$u = -K\frac{\partial(z+h)}{\partial x}, \tag{2a}$$

$$v = -K\frac{\partial(z+h)}{\partial y}, \tag{2b}$$

$$K = \frac{h}{H}K_S; \tag{2c}$$

$$\frac{\partial Q}{\partial s} + \frac{\partial A}{\partial t} = \frac{I_e \cdot dx \cdot dy}{ds}, \text{ with } Q \geq 0,\ A \geq 0; \tag{3}$$

$$Q = n^{-1}F^{2/3}i^{1/2}A^m; \tag{4}$$

where t is time; x and y, orthogonal coordinate axes in the horizontal plane; u and v, Darcy velocities in x and y directions; z, elevation of the impermeable layer; K, soil hydraulic conductivity; $n_e = \phi - \theta_{33}$, drainable porosity; s, longitudinal coordinate of the open channel network; Q, surface flow discharge; A, surface flow cross-sectional area; i, channel bed slope; n, Manning's roughness; F, shape factor in the expression for the hydraulic radius equal to $F \times A^{1/2}$ [*Grayson and Bloschl*, 2000]. In accordance with Dupuit's approximation, equations (1a), (2a), and (2b) are the mass and momentum conservation equations for 2-D saturated subsurface flow. To model vertical heterogeneity of soil with hydraulic conductivity decreasing with depth [*Beven*, 1984], the equation (2c) is used, where K_S is the saturated hydraulic conductivity at the surface. In accordance with the Saint-Venant equations and the kinematic approximation, equations (3) and (4) are the mass and momentum conservation equations for 1D gradually varied surface flow.

3. Finite Difference Schemes for Surface and Subsurface Flow

[8] The partial differential equations (1)–(4) for surface and subsurface flow are solved by conventional finite difference schemes. The same numerical discretization is considered for the soil and channel flow components, with time step Δt and uniform spatial steps $\Delta s = \Delta x = \Delta y$. Space cells of grid DEM and the other landscape parameters have also been set as equal to this size. For the 2-D subsurface flow, by combining equations (1) and (2) and substituting the variable h with the new dependent variable $\zeta = n_e h$, the solution equation, written in finite difference form for the internal element (i, j) of the computational space-grid and the time level $n + 1$, is

$$\zeta_{i,j}^{n+1} = \zeta_{i,j}^{n} + \frac{\Delta t}{4\Delta s^2}\left(f_{i+1/2,j} - f_{i-1/2,j} + f_{i,j+1/2} - f_{i,j-1/2}\right)^n + \Delta t(P_e - ET - I_e)_{i,j}^{n+1}, \tag{5a}$$

with

$$f_{k+1/2}^{n} = \frac{(K_{Sk+1} + K_{Sk})}{(H_{k+1} + H_k)}\left(\frac{\zeta_{k+1}^n}{n_{ek+1}} + \frac{\zeta_k^n}{n_{ek}}\right)^2 \cdot \left(z_{k+1} + \frac{\zeta_{k+1}^n}{n_{ek}} - z_k - \frac{\zeta_k^n}{n_{ek}}\right). \tag{5b}$$

Equation (5) is obtained using a one-step, explicit, time forward, and space-centered 2-D scheme. The simple scheme used is not unconditionally stable, but the small values of soil hydraulic conductivity meet the necessary Courant condition for explicit schemes [*Abbott*, 1992; *Weiyan*, 1992]. This explicit scheme does, however, have the advantage of reducing the amount of computer time and core storage, as these tend to increase greatly with basin size and with decreasing space and time steps. The space and time steps size must, indeed, be small enough to meet the accuracy requirement of the difference solution.

[9] For the 1D surface flow the mass conservation equation (3), written in finite difference form for the channel network link between the upstream grid node i and the downstream grid node $i + 1$, is

$$\frac{\lambda\left(Q_{i+1}^{n+1} - Q_i^{n+1}\right) + (1-\lambda)\left(Q_{i+1}^{n} - Q_i^{n}\right)}{\Delta s} + \frac{\left(A_{i+1}^{n+1} - A_{i+1}^{n}\right) + \left(A_i^{n+1} - A_i^{n}\right)}{2\Delta t} = I_{ei+1}^{n+1} \cdot \Delta s. \tag{6}$$

Equation (6) is obtained using the weighted four-point implicit finite difference scheme [*Fread*, 1993], where the space-weighting discretization coefficient is set to 0.5. The value of the time-weighting coefficient $\lambda = 0.6$ is used to prevent conditions of instability in the centered scheme ($\lambda = 0.5$), and to decrease the numerical dissipation of the unconditionally stable fully implicit scheme ($\lambda = 1$). The application of this scheme is based on the spatial structure of the channel network extracted from the grid DEM by an automatic procedure which makes use of Operational Research algorithms for "network flows" [*Niedda*, 1996]. The connected tree structure of the channel network is stored in vector form with graph techniques, which are very efficient for large networks as they reduce computer time and optimize memory storage [*Niedda and Sechi*, 1996]. Equations (4) and (6) are combined and solved starting from the upstream nodes, where the boundary condition $Q_0 = 0$ is assigned, and following the connected tree network down to the root node.

4. Study Catchments

[10] Two case studies are presented, showing the application of the model to two steep forested catchments with thin soil layers, one medium-sized and one small-sized. Both the catchments are situated in a mountainous area in the center of Sardinia, Italy, as shown in Figure 2. The area has a temperate Mediterranean climate with highly variable rainfall, mainly concentrated in winter. In both the forested catchments the dominant hydrologic response is runoff from saturated source areas.

4.1. Basin 1

[11] The first application is to the 4.56 km^2 Ortobene catchment. The river basin ranges in altitude from 950 to 180 m above sea level, with an average of 520 m, and an average surface slope of 34.4%. Three digital maps were created for elevation, soil type and land use (Figures 2a, 2b, and 2c). The contour lines for elevation intervals of 25 m were digitized from 1:10,000 scale maps. Soil maps were obtained from soil surveys and from 1997 aerial photographs. Land use in the upper part of the basin consists

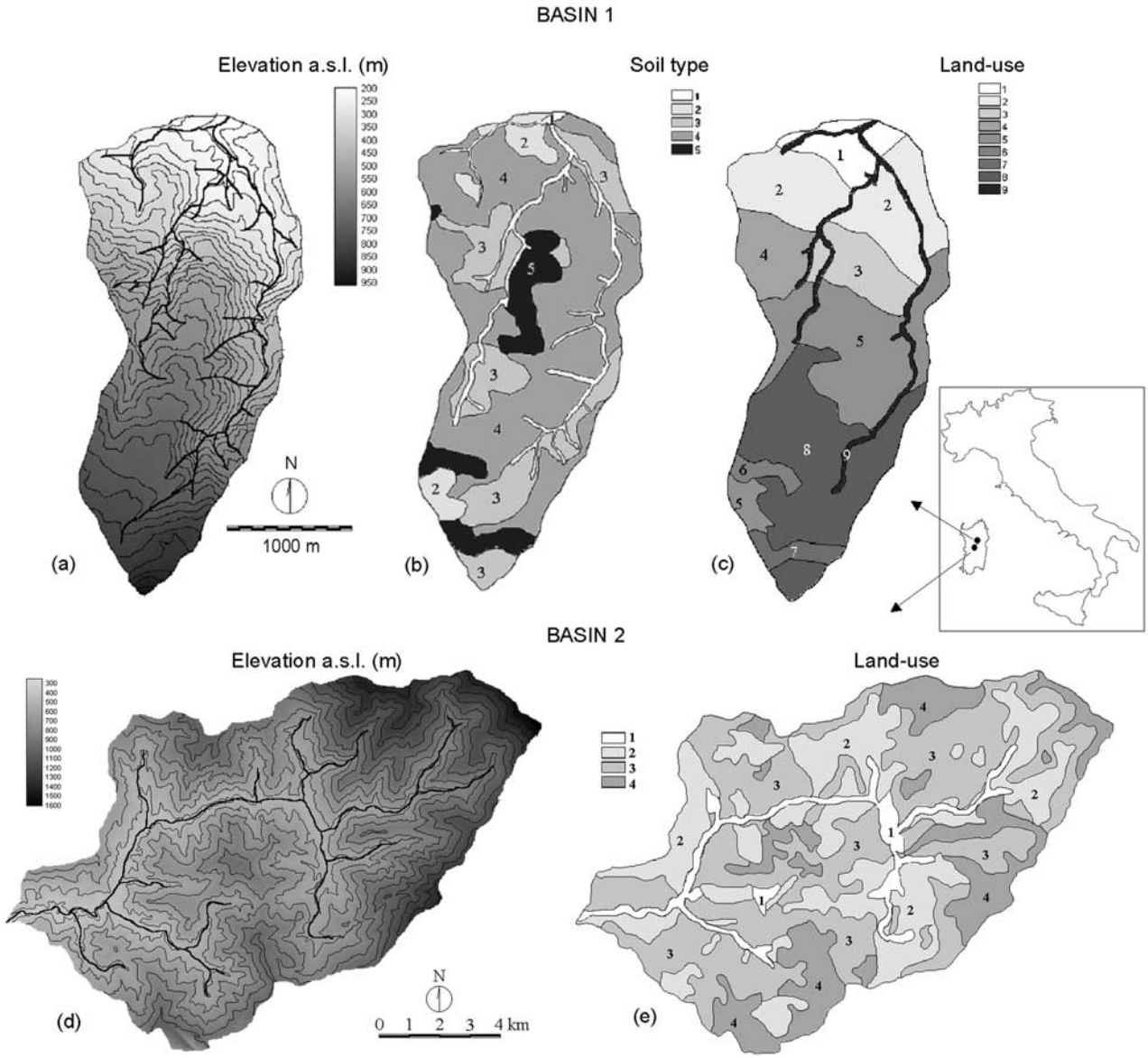

Figure 2. The two study catchments in Sardinia, Italy. The 4.56-km^2 basin 1 (40.3°N, 9.4°E): (a) digital elevation model and channel network; (b) map of surface soil type; (c) map of land use. The 123-km^2 basin 2 (40°N, 9.2°E): (d) digital elevation model and channel network; (e) map of land use and surface soil type.

mainly of a forest of Holm-oaks, and in the lower part mainly of Mediterranean maquis. The basin is not urbanized and the only cultivated area is near the basin outlet. The dominant soil type is loamy sand, overlying bedrock of Paleozoic granite, as shown in Table 1. Soil ranges in thickness from 20 to 60 cm. Along the channel network there are alluvial deposits which are between 60 and 120 cm in depth. The texture of this soil type is sandy clay loam with large deposits of coarse aggregate.

[12] Rainfall and streamflow data collection began within the basin in Spring 2000. The runoff was monitored in the basin outlet with an area-velocity flowmeter consisting of two integrated sensors. These measured the water level and the depth-averaged velocity. The cumulative rainfall and the outlet discharge in the monitoring period are shown in Figure 3a. There were only two intense rainfall events of 77 and 42 mm. There was a loss of runoff data during the first intense rainfall event due to a power failure.

4.2. Basin 2

[13] The second application is to the 123 km^2 Araxisi catchment. It ranges in altitude from 1600 to 350 m above sea level, with an average of 804 m, and an average surface slope of 33.8%. Digital maps were created for elevation, soil type and land use (Figures 2d and 2e). The contour lines at 25 m intervals were digitized from 1:25,000 scale maps. According to soil surveys and aerial photographs, land use consists partly of natural pasture with scrub and partly of deciduous hardwood forest, and there are very few urbanized and crop-growing areas. The dominant soil type is sandy loam of recent alluvial origin, overlying impermeable bedrock consisting mainly of metamorphic schist, and, to a

Table 1. Soil and Land Use Properties for Basin 1

	Soil Type[a]				
	1	2	3	4	5
Texture	sandy clay loam	sandy loam	loamy sand	loamy sand	loamy sand
Relative area	0.07	0.05	0.22	0.55	0.11
Drainable porosity	0.143	0.246	0.312	0.312	0.312
Soil water content at −33 kPa	0.255	0.207	0.125	0.125	0.125
Saturated hydraulic conductivity, mm/h	120	30	60	60	60
Soil thickness, m	0.9	0.6	0.5	0.4	0.2

	Land Use[b]								
	1	2	3	4	5	6	7	8	9
Surface cover	tillage	pasture + scrub	dense scrub	scrub + rock	scrub + grass	urbanized + grass	grass + rock	holm-oaks	riparian vegetation
Relative area	0.05	0.25	0.09	0.06	0.19	0.01	0.02	0.27	0.05
Leaf area index	3	3	2	1.25	2.5	1	1	10	3

[a]See Figure 2b.
[b]See Figure 2c.

lesser extent, granite. Soil thickness ranges mainly from 20 to 50 cm, as shown in Table 2. Alluvial deposits are found along streams in valley bottoms and range in thickness from 100 to 150 cm.

[14] The Araxisi catchment has been monitored by the National Hydrographic Institute since 1934. The average monthly temperatures range from a maximum of 25°C in July and August to a minimum of 3°C in January and February. There is a rain gage inside the basin at 920 m above sea level and a stream gage at the basin outlet. The average annual rainfall is 1000 mm. Annual streamflow in the basin outlet is on average 350 mm, ranging from minimum values below 70 mm to maximum values above 600 mm, and tends to dry up altogether during the summer period. For these stations time data is available at 15 min intervals for the years 1947–1983, with, however, some data missing for certain periods. In a preceding work, continuous simulation was carried out using the data sequence 1947–1958 [*Niedda*, 2000]. This sequence was selected because it was the one with least data missing. For the present analysis the hydrological years 1956–1957, with different mean flood events, and 1947–1948, with the major flood event, were selected. The cumulative rainfall and the outlet discharge in these two years are shown in Figures 3b and 3c.

5. Model Parameterization

[15] The input parameters were landscape topography, channel network, climatic inputs, land use and soil properties. The problem of subcatchment variability was solved by dividing the basin into domains of uniform combinations of land use and soils. Since equation variables and parameters were defined on a space-grid system, the surface and soil properties were assigned to each grid cell by the vector-to-raster operation. Idrisi32 Geographical Information System software was employed to convert vector lines to raster DEMs. A 3 × 3 mean filter was applied to the elevation of each pixel, to remove some of the angularity of the linear interpolation of the digitized lines, as is strongly recommended by the suppliers.

[16] The soil water content at −33 kPa matric potential θ_{33}, the drainable porosity $n_e = \phi - \theta_{33}$ and the saturated hydraulic conductivity values reported in Tables 1 and 2 were assigned to the basin domains of the uniform soil types shown in Figures 2b and 2e, respectively. These were estimated from soil texture [*Rawls et al.*, 1993], choosing the average value of numerous representative laboratory measurements. A correction was made to the saturated hydraulic conductivity value of soil type 1, in order to take into account the large quantity of coarse aggregate in the alluvial deposits found in the valley bottom along the channel network. Manning's roughness coefficient $n = 0.05\ \mathrm{m}^{-1/3}\mathrm{s}$ from the literature for mountain streams was chosen for the two catchments, together with $m = 4/3$ and $F = 0.25$ for trapezoidal channel flow.

[17] Actual evapotranspiration (ET) was calculated from the reference potential evapotranspiration (PET) as follows:

$$\mathrm{ET} = K_w\, K_c\, \mathrm{PET}, \tag{7}$$

where $K_w = \theta/\theta_{33}$ if $\theta < \theta_{33}$, or if not, $K_w = 1$, and K_c being a crop coefficient which integrates all the effects of the characteristics that distinguish the land use from the reference crop. The crop coefficient was obtained during the calibration procedure as fitting parameter. For basin 1 the potential evapotranspiration with a daily time step (Figure 3a) was estimated using the modified FAO Penman-Monteith method [*Allen et al.*, 1998]:

$$\mathrm{PET} = \frac{0.408\Delta(R_{ns} + R_{nl} - G) + \gamma \frac{900}{T+273} u_2 (e_s - e_a)}{\Delta + \gamma(1 + 0.34u_2)}\ (\mathrm{mm/day}), \tag{8}$$

where R_{ns} and R_{nl} are net shortwave and longwave radiation at the crop surface in (MJ m^{-2} day^{-1}); G, soil heat flux density in (MJ m^{-2} day^{-1}); T, mean daily air temperature in (°C) at 2 m height; u_2, wind speed at 2 m height; $(e_s - e_a)$, saturation vapor pressure deficit in (kPa); Δ, the slope of the vapor pressure-temperature curve in

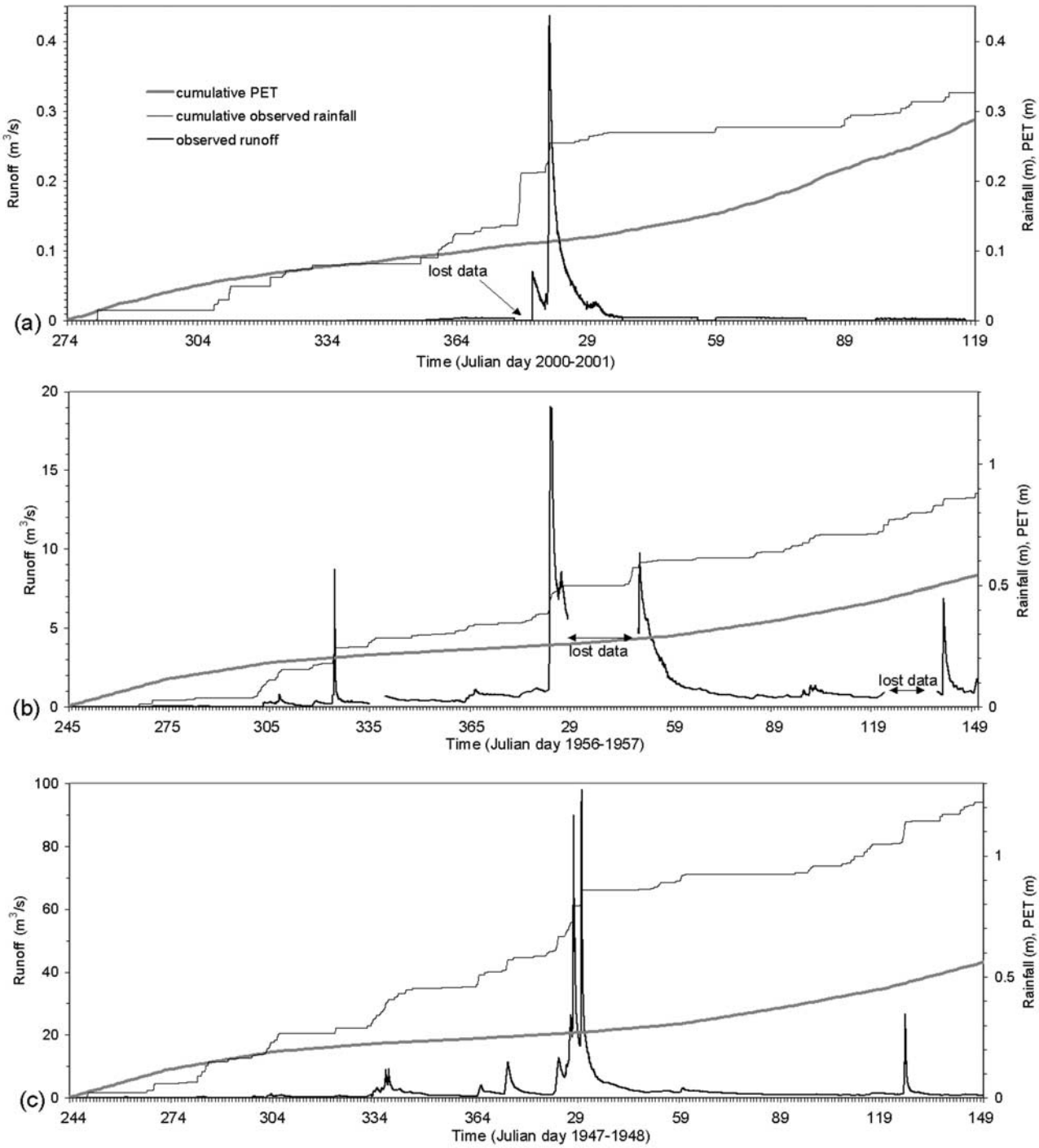

Figure 3. Discharge monitored at the basin outlet, cumulative rainfall and reference potential evapotranspiration (PET) (a) for basin 1 and (b and c) for basin 2.

(kPa $°C^{-1}$); γ, the psychrometric constant in (kPa $°C^{-1}$). Equation (8) was applied using the daily climatic data (air temperature, relative humidity, global solar radiation and wind speed u_2) monitored in the nearest climate station which is 9 km from basin 1. Maximum, mean and minimum air temperatures and maximum and minimum relative humidity were used to estimate $(e_s - e_a)$, G and R_{nl}. Global solar radiation was used to estimate R_{ns}, with an albedo of 0.23, and R_{nl}. For basin 2 the only climatic data available was the temperature. Consequently the potential evapotranspiration was estimated with the temperature-based Hargreaves equation: $PET = 0.0023 \cdot S_0 \sqrt{\Delta T}(T + 17.8)$, with a monthly time step, where ΔT is the difference between mean monthly maximum and minimum temperatures, and S_0 is the water equivalent of extraterrestrial solar radiation. The computed evapotranspiration (Figures 3b and 3c) was distributed uniformly over the month.

Table 2. Soil and Land Use Properties for Basin 2

	Soil Type and Land Use[a]			
	1	2	3	4
Texture	sandy loam	sandy loam	sandy loam	sandy loam
Relative area	0.07	0.3	0.44	0.19
Drainable porosity	0.246	0.246	0.246	0.246
Soil water content at −33 kPa	0.207	0.207	0.207	0.207
Sat. hydraulic conductivity, mm/h	120	30	30	30
Soil thickness, m	1.5	1	0.5	0.2
Surface cover	riparian vegetation	scrub + pasture	hardwood	hardwood
Leaf area index	3	3	7	7

[a]See Figure 2e.

[18] The interception storage capacity S was determined from the leaf area index (LAI):

$$S = H_r \, \mathrm{LAI}, \tag{9}$$

where H_r is the rainfall interception coefficient, set to 0.2 mm/LAI [*Dickinson et al.*, 1991]. The values of LAI (Tables 1 and 2) were estimated for each surface cover [*Dingman*, 1994], and were assigned to the uniform land use domains shown in Figures 2c and 2e. The evaporation rate of intercepted water E was obtained during the calibration procedure as fitting parameter. Since there was no detailed information on the atmospheric conditions and vegetation, a seasonal value for parameter E could not be defined.

6. Calibration and Sensitivity Analysis

[19] Although this study is not specifically concerned with assessing the performance of a watershed model, it was of great importance that the simulations be realistic. Fit process calibration was applied first, based on visual inspection of simulated hydrographs and quantification of goodness of fit. This was evaluated by means of the coefficient of efficiency (EF), as used by *Nash and Sutcliffe* [1970]:

$$\mathrm{EF} = 1 - \left[\sum_{t=1}^{N} \left(Q_o(t) - Q_s(t)\right)^2\right] \cdot \left[\sum_{t=1}^{N} \left(Q_o(t) - \overline{Q_o}\right)^2\right]^{-1}, \tag{10}$$

where Q_o and Q_s indicate the observed and simulated discharges, respectively, and the overbar denotes the mean for the entire simulation period divided into N time steps. The initial model setup was developed using the time step Δt = 900 s and the space steps Δs = 5 m for the smaller basin 1 and Δs = 25 m for the larger basin 2. Grid DEMs and the other input grid maps were sampled for these sizes. The simulation was run from October 2000 to April 2001 for basin 1, and from September 1956 to May 1957 and from September 1947 to May 1948 for basin 2. These three hydrological years involve three different flood runoff scales, respectively of 0.5, 20, and 100 m^3/s. The soil of the two basins was considered completely dry as an initial condition, as there had been a drought in the previous months, with no rainfall whatsoever. Three parameters were used in the calibration process: the crop coefficient K_c, the evaporation rate from interception storage E, and the effective hydraulic conductivity K_S obtained with the formula:

$$K_S = \alpha \cdot K_S^*, \tag{11}$$

where K_S^* is the value derived from soil texture and α is a fitting amplification factor. The comparisons of the observed and simulated outlet discharge for the two catchments are shown in Figure 4. The optimized parameter values and the simulation efficiency coefficients are reported in Table 3. The efficiency for basin 2 varied from EF = 0.87 in the year 1956–1957 with an evaporation rate of E = 0.4 mm/h, to EF = 0.78 in the year 1947–1948 with E = 0.6 mm/h. The difference in these evaporation values and the value E = 0.95 mm/h for basin 1 may be due to the different temperatures, and to the different altitude of the two basins. The difference is, however, great, and its magnitude may be due to the fact that this calibration parameter compensates for the measurement errors and the errors caused by the lack of detailed information on the climate and vegetation. The conductivity amplification factors α = 15 and 25 for the two catchments seem high. In this respect in many dynamic physically based hydrologic models, the soil hydraulic conductivity resulting from field measurements was increased by one order and more, up to 1000 mm/h, to improve the efficiency of the simulation [see, e.g., *Grayson et al.*, 1992a; *Paniconi and Wood*, 1993; *Wigmosta et al.*, 1994]. This very high effective hydraulic conductivity may be due to scale effects in topographic discretization, to numerical dissipation of the finite difference scheme used for the subsurface flow equation and to other factors, such as macropores, whose effects may not be captured in a point measurement but are evident at larger scales. The main goal of this work is to increase our understanding of the spatial resolution effects on the scale parameterization problem in a numerical routing. This is investigated in the next section.

[20] A univariate analysis procedure was employed to investigate the sensitivity of the model parameters. Each parameter was varied one at a time, within a range of physically realistic values (Table 4), while the other input parameters were kept at the value defined in the parameterization and calibration process. The relative influence of each parameter was evaluated with mean absolute difference

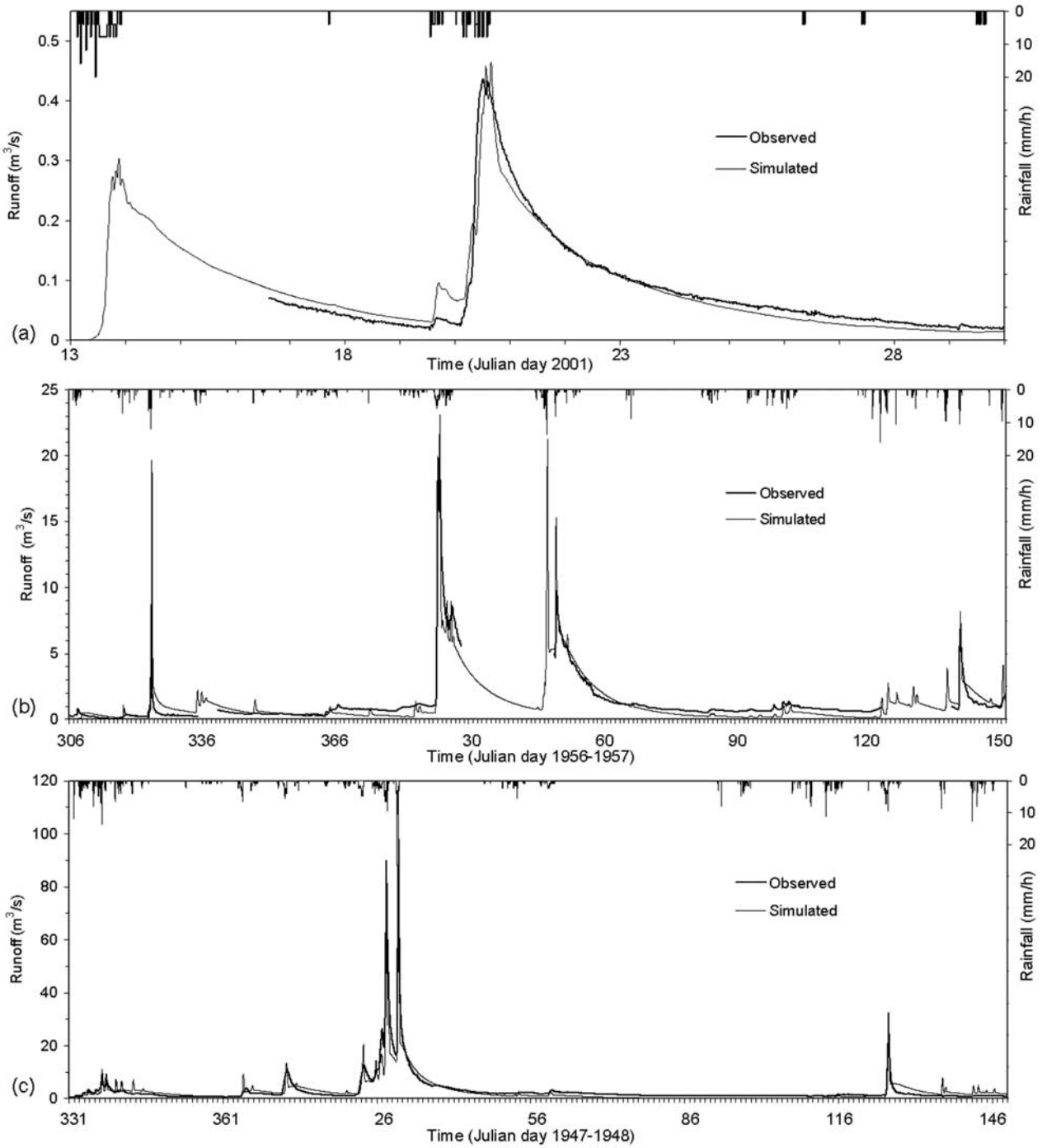

Figure 4. Comparison of observed and simulated discharge hydrographs and observed rainfall: (a) for basin 1 and (b and c) for basin 2.

(MAD) (12a) and with Pearson's product moment correlation coefficient r(12b):

$$\mathrm{MAD} = N^{-1} \sum_{t=1}^{N} |Q_L(t) - Q_U(t)|, \tag{12a}$$

$$r = \left[\sum_{t=1}^{N} \left(Q_L(t) - \overline{Q_L}\right)\left(Q_U(t) - \overline{Q_U}\right) \right] \cdot \left[\sum_{t=1}^{N} \left(Q_L(t) - \overline{Q_L}\right)^2 \right]^{-0.5} \cdot \left[\sum_{t=1}^{N} \left(Q_U(t) - \overline{Q_U}\right)^2 \right]^{-0.5}. \tag{12b}$$

Table 3. Time and Space Steps, Fitting Parameters (Crop Coefficient, Evaporation Rate From Interception Storage, and Conductivity Amplification Factor), and Efficiency Coefficient of the Continuous Hydrologic Simulation.

Basin	Surface, km^2	Mean Altitude, m asl	Simulation Year	Time Step, s	Space Step, m	Fitting Parameters			
						K_c	E, mm/h	α	Efficiency
1	4.56	520	2000–2001	900	5	1	0.95	15	0.95
2	123	804	1956–1957	900	25	0.5	0.4	25	0.87
2	123	804	1947–1948	900	25	0.5	0.6	25	0.78

Table 4. Univariate Sensitivity of the Model Parameters

Domain	Parameter	Description	Range	Basin 1		Basin 2	
				MAD, m^3/s	r^2	MAD, m^3/s	r^2
Land	H_r	rainfall interception coefficient (mm/LAI)	0.1–0.3	0.044	0.9	0.373	0.97
Land	E	evaporation of intercepted water (mm/h)	0.4–1	0.053	0.94	0.729	0.77
Land	K_c	crop coefficient	0.5–1	0.032	0.88	0.428	0.91
Soil	θ_{33}	soil water content at −33 kPa	0.12–0.30	0.06	0.66	0.518	0.95
Soil	n_e	drainable porosity	0.15–0.35	0.063	0.58	0.544	0.82
Soil	α	conductivity amplification factor	10–50	0.049	0.78	0.531	0.78
Channel	n	Manning's roughness coefficient ($m^{-1/3}s$)	0.02–0.10	0.008	0.91	0.191	0.72
Channel	λ	time-weighting discretization coefficient	0.6–0.9	0.001	1	0.015	1
Channel	m	coefficient for channel-overland flow	1.33–1.67	0.004	1	0.041	1
Channel	F	coefficient for channel-overland flow	0.25-Δs^{-1}	0.004	1	0.041	1
Grid	Δs	space step (m)	1 order	0.05	0.18	0.73	0.45
Grid	Δt	time step (s)	90–900	0.005	1	0.015	1

These were computed between the two outlet discharge series Q_L and Q_U, simulated by using the lower and the upper bounds of the parameter range, respectively. As reported in Table 4, subsurface flow parameters were those with the highest absolute differences and the lowest correlation coefficients, with respect to surface flow and land use parameters. The high sensitivity of the soil parameters was expected for this kind of modeling, which is based on runoff production from saturated source areas. The sensitivity of these parameters is high not only for base flows near the mean, as can be seen from the high MAD values, but also for the extreme events, as is evidenced by the low values of r^2, this correlation measure being more sensitive to outliers [*Legates and McCabe*, 1999]. As expected, the evaporation coefficients showed greater sensitivity for base flows, and the channel roughness coefficient was only highly sensitive for extreme flows. Higher sensitivity, however, was shown for the space-grid size, which varied between 5 and 50 m for basin 1, and 25 and 250 m for basin 2. Sensitivity to time discretization, by contrast, was negligible between the steps of 90 and 900 s for these specific model applications. The evidence of this scale dependence confirms that the effects of grid size and numerical resolution on watershed simulation need to be investigated more thoroughly.

7. Grid Scale and Numerical Resolution Investigation

[21] Different space-grid sizes were used to investigate grid scale and numerical resolution effects on simulated runoff. The DEMs and the other input maps were sampled for grid sizes of 5, 10, 25, and 50 m for the smaller basin 1, and 25, 50, 100, and 250 m for the larger basin 2. To investigate the effects of both the topography resolution and the finite difference scheme dissipation separately, the coarse-grid DEMs were subdivided using finer nested grids. The elevation of each cell of the finer nested grid was calculated by bilinear interpolation of the elevations of the neighboring four coarse-grid points, as shown in the example of Figure 5. The DEMs thus generated have the same topography resolution as the original coarse-grid DEM even though their cells are smaller. In the following sections the cell size of the interpolated DEM defines the space step Δs of the numerical scheme. The cell size of the original DEM defines the topography resolution R. All the DEMs of the finer grids (up to Δs = 5 m for basin 1 and Δs = 25 m for basin 2) were generated by interpolation of DEMs with resolution R = 10, 25, and 50 m for basin 1, and R = 50, 100, and 250 m for basin 2. By using these DEMs, the numerical scheme was run with space steps smaller than topography resolution ($\Delta s < R$). Obviously the numerical scheme cannot consider topography resolutions finer than the space step. Simulations were first run at a number of different topography resolutions, but using the same (small) space step, to study the grid-scale effects independently from the numerical dissipation. Simulations were then run at a number of different space steps, but using the same (coarse) topography resolution to study the effects of numerical scheme dissipation.

7.1. Topography Resolution Effects on Flow Routing

[22] The grid-scale effects were studied by comparing the simulated runoff responses for different topography discretizations, but using the same space step of the numerical scheme. The model with topography resolutions R = 5, 10, 25, and 50 m for the smaller basin 1, and R = 25, 50, 100, and 250 m for the larger basin 2, was run with space steps Δs = 5 m for basin 1, and Δs = 25 m for basin 2. The simulations were carried out using the parameter values

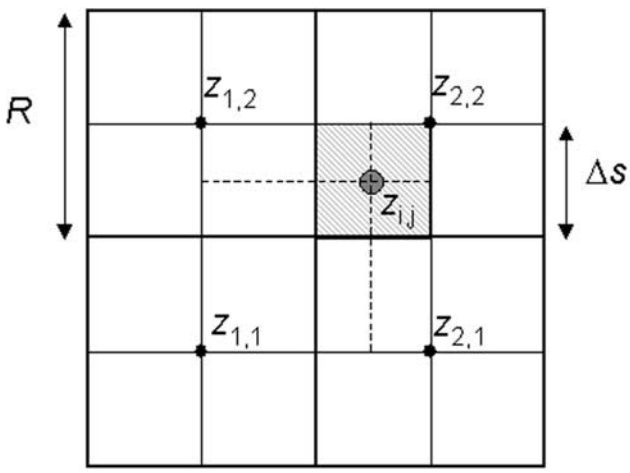

Figure 5. An example of a fine nested grid DEM generated by a coarser grid DEM, with resolution R and cell size $R/2$. The elevation of the generated DEM is calculated by bilinear interpolation of the elevations of the neighboring four coarse grid points.

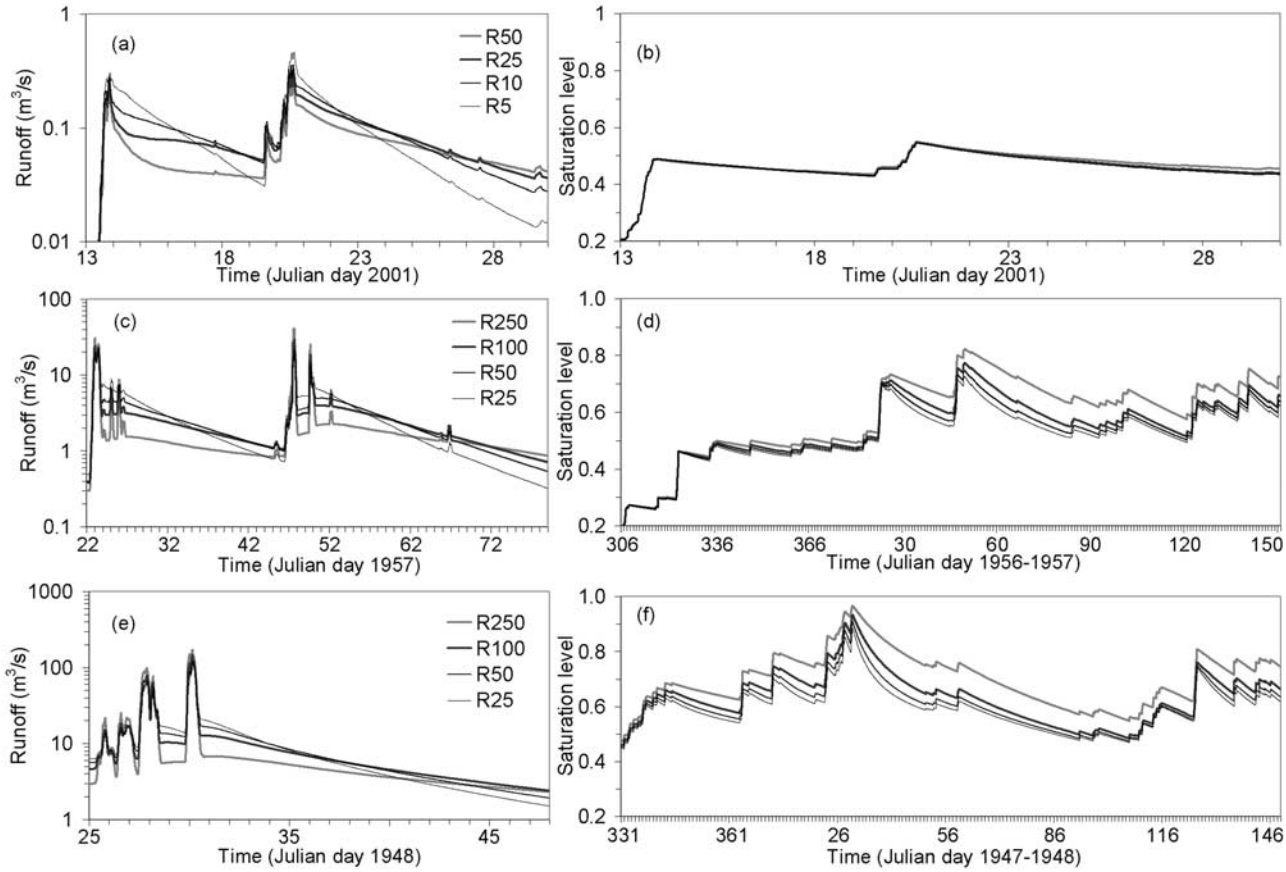

Figure 6. Simulated discharge hydrographs and saturation level (total soil moisture to soil porosity) obtained for different topography resolutions R, adopting the same space step of the numerical scheme and the same hydraulic conductivity: (a and b) for basin 1 with R = 5, 10, 25, and 50 m and (c, d, e, and f) for basin 2 with R = 25, 50, 100, and 250 m.

already obtained in the calibration process. The simulated discharge hydrographs during the major flood events and the consequent recessions are shown in Figures 6a, 6c, and 6e for the two study catchments. The comparison of the recession curves governed by the subsurface flow highlights that, if the same value of hydraulic conductivity is used, the rate of decay decreases in all the simulations as the topography resolution becomes coarser. Thus coarser topography produces slower subsurface flow response. With a slower flow rate, the soil moisture decreases more slowly, as shown in Figures 6b, 6d, and 6f for the two study catchments, where the saturation level (soil moisture to soil porosity) of the whole basin is represented. Thus coarser topography resolution may result in higher soil moisture and a rainfall event may cause higher peak discharges, as can be seen from the hydrographs for the basin 2 (Figures 6c and 6e). This is not the case of the hydrograph for the basin 1 (Figure 6a), as it relates to the first flood event and the low antecedent moisture conditions are the same for the different resolutions (Figure 6b).

[23] A calibration procedure was then applied to optimize the values of hydraulic conductivity for each topography resolution, in order to obtain the same recession curves for the simulated and observed discharge hydrographs. The response hydrographs obtained in this way for the two study catchments and the three years simulated show very similar recession curves for each grid resolution, as shown in Figures 7a, 7c, and 7e. The fitting values of the conductivity amplification factor α for each grid resolution are shown in Figure 8a. As expected, these values increase with increasing grid size. There are still some differences in the detailed flow process within a storm event, which is also governed by the channel flow routing model, as shown in Figures 7b, 7d, and 7f. A plot of the simulated to observed peak discharge versus grid resolution is shown in Figure 8b. The simulated peak discharges decrease with increasing grid size, which correlates with the evidence that coarse topography produces a slower flow rate.

7.2. Numerical Scheme Dissipation

[24] The simulated runoff responses for different space steps of the numerical scheme were compared using the same coarse topography resolution. The model with space steps Δs = 5, 10, 25, and 50 m and resolution R = 50 m was run for basin 1, and with space steps Δs = 25, 50, 100, and 250 m and resolution R = 250 m for basin 2. The simulations were carried out using the parameter values already obtained from the calibration process (conductivity amplification factor α = 75 with R = 50 m for basin 1, α = 200 with R = 250 m for basin 2). The discharge hydrographs and the resulting recession curves during the major flood events of the three simulated years are shown for the two study catchments in Figure 9. The simulated hydrographs show very similar recession curves for each space step used.

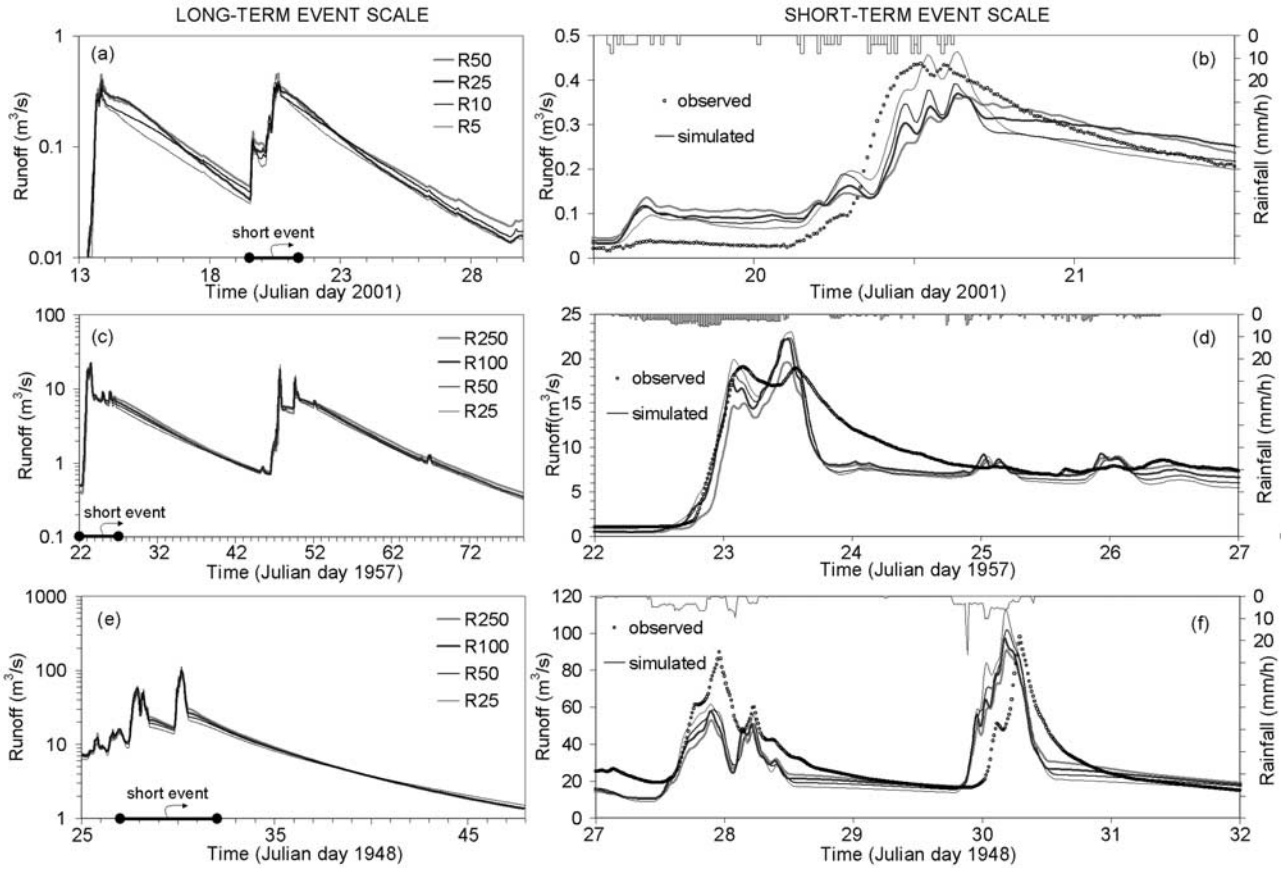

Figure 7. Comparison of simulated discharge hydrographs obtained with the hydraulic conductivity values optimized for the different topography resolutions R and adopting the same space step of the numerical scheme: (a and b) for basin 1 with R = 5, 10, 25, and 50 m and (c, d, e, and f) for basin 2 with R = 25, 50, 100, and 250 m.

This suggests that the numerical dissipation of the finite difference scheme used for the 2-D subsurface flow does not have scale effects on soil conductivity estimation in the space discretization range of this application test. By contrast there are remarkable differences in the detailed flow process within a storm event, which is also governed by the kinematic channel flow routing model, as shown in Figures 9b, 9d, and 9f. The accuracy of simulation of the flood discharges decreases when large space steps are used. Indeed, hydrograph examination in both the basins reveals that, as the space step increases, a faster response with higher peak discharges with respect to observed data, is linked to a slower response immediately after the peak discharge. This flashier response of the numerical scheme

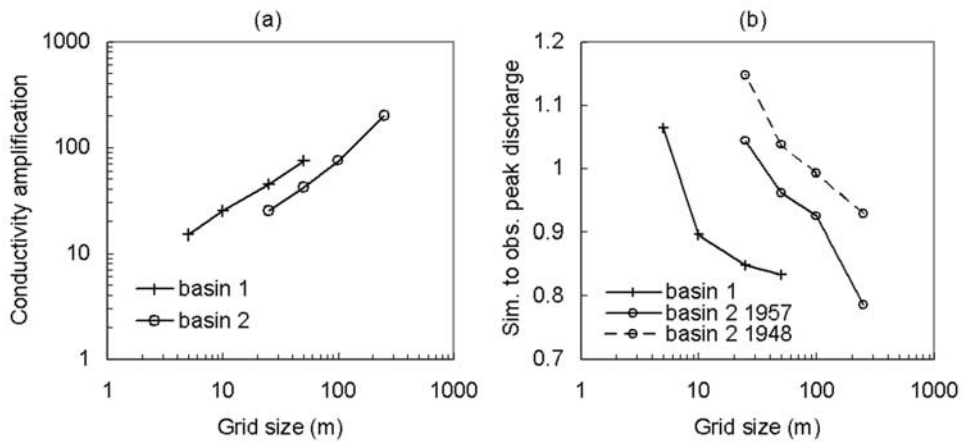

Figure 8. (a) Optimized values of the hydraulic conductivity amplification factor and (b) simulated to observed peak discharge versus topography resolution for the two catchments.

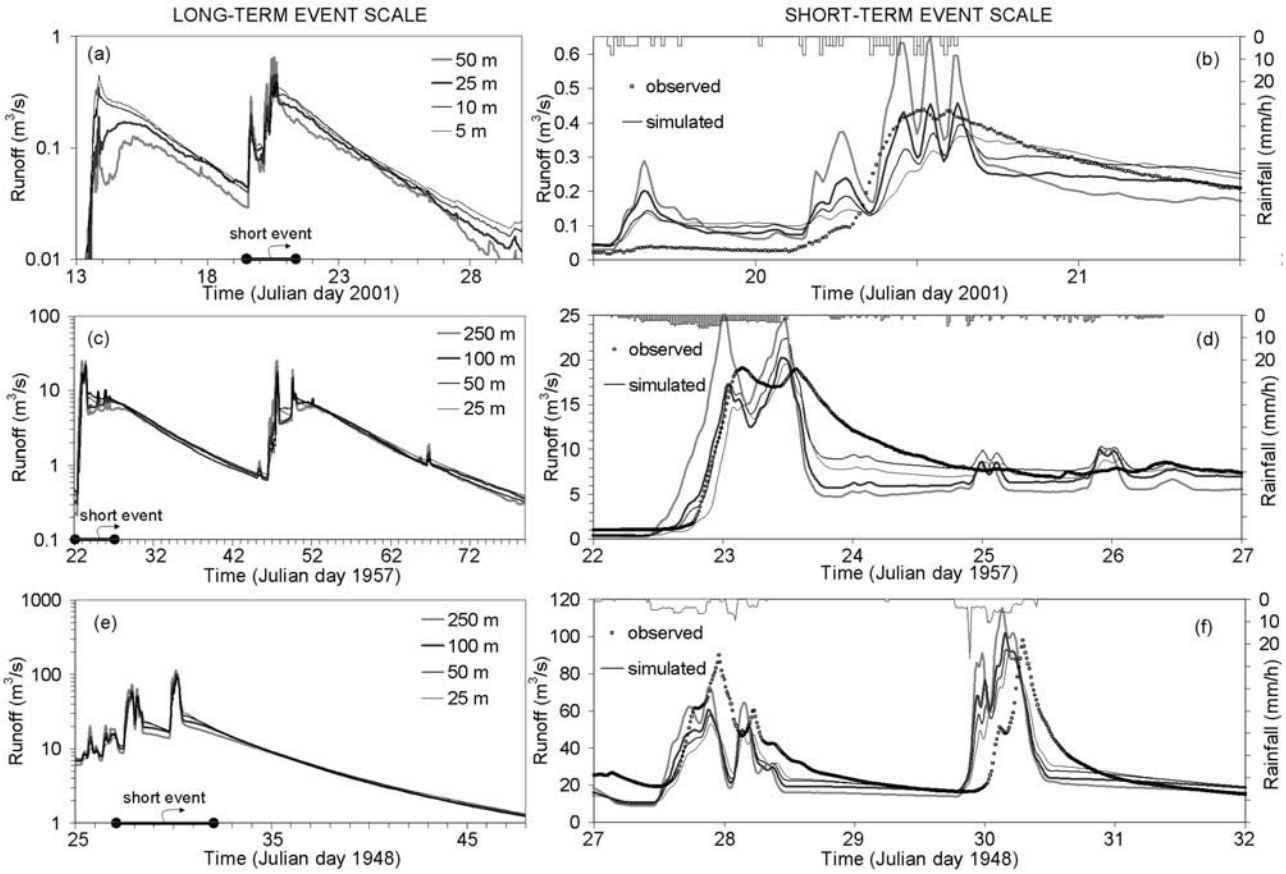

Figure 9. Comparison of simulated discharge hydrographs obtained for different space step of the numerical scheme adopting the same topography resolution-hydraulic conductivity: (a and b) for basin 1 with steps of 5, 10, 25, and 50 m and (c, d, e, and f) for basin 2 with steps of 25, 50, 100, and 250 m.

could be due to the distributed model not accurately simulating the extension of the stream network during a rainfall event. This may be a result of the subsurface flow finite difference scheme. The model is based on the "saturation excess" mechanism of runoff production from variable source areas and the extension of the stream network along valley bottoms is determined by this scheme.

[25] As can be seen from the simulation tests, the saturated source areas are larger and are found nearer the basin outlet when the spatial grid size increases, so the runoff response is flashier. With larger grid sizes, along valley bottoms these areas are wider (the minimum width may not be less than the grid size), but shorter (stream network is less expanded). By contrast as the spatial grid size decreases, the saturated areas are narrower and longer, and represent the stream network more accurately (stream network is more expanded). The flow paths and the travel time of surface flow are longer, the drainage from the saturated zones near the channel system is greater, and thus the channel response is more damped.

8. Spatial Aggregation and Information Content

[26] Since the subsurface flow equation is a function of landscape curvature and slope gradient, the change in the rate of flow response with topography resolution may come from these topographic factors being misrepresented, above all in steep basins. As grid size increases the slope and curvature of the watershed are generally reduced, because elevation values are averaged within each cell. This spatial aggregation produces a smoother relief, resulting, at the limit, in the null slope of a uniform altitude landscape. The reduction of curvature and slope gradient with spatial aggregation is thus the source of many errors in watershed simulation and parameter estimation. Cumulative frequency distributions of slope and profile curvature were calculated for each DEM of the two study catchments. As shown in Figure 10, grid size significantly affects the frequency distributions. This agrees with the results of *Zhang and Montgomery* [1994]. In both the basins, as grid size increases the slope is proportionally reduced in all the frequency classes. By contrast the profile curvature is severely reduced in its higher values.

[27] The concept of loss of information content [*Vieux*, 1993; *Singh*, 1997] was used in this work to describe the effect of spatial aggregation on the topographic parameters derived from DEM for different grid sizes. The information content I, as variability measure of the spatial distribution of a parameter, is defined by the following relationship:

$$I = -\sum_{j=1}^{N} p_j \ln(p_j), \tag{13}$$

where N is the number of bins into which the parameter range is divided and p_j is the proportion of elements in the

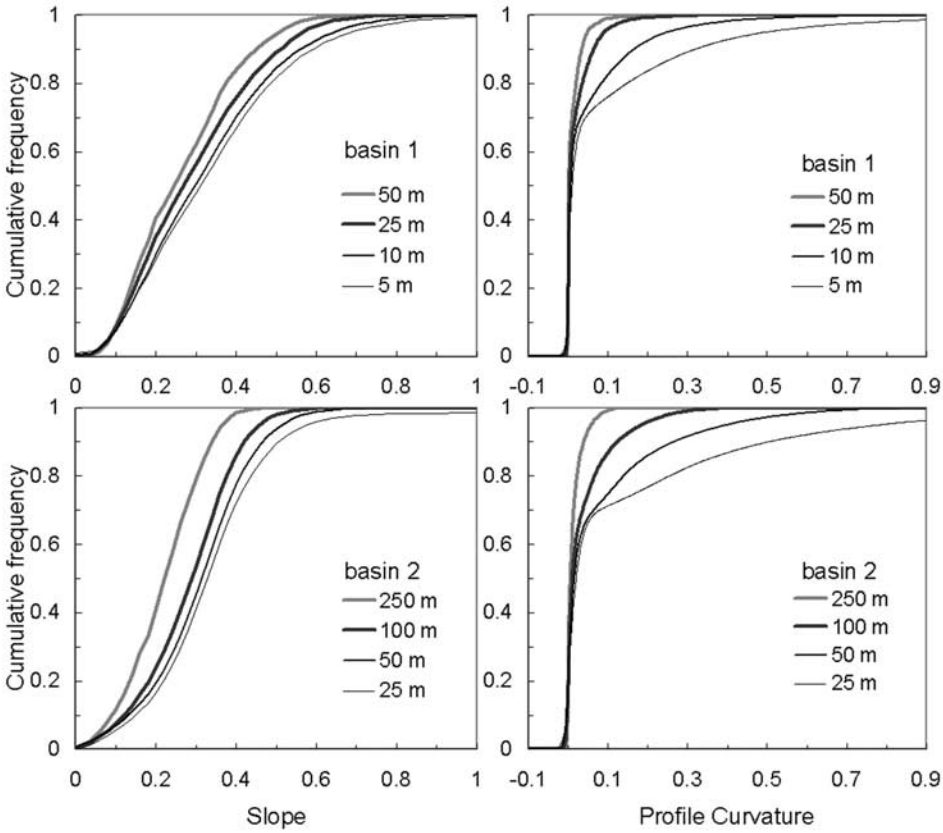

Figure 10. Cumulative frequency distributions of slope (bins 0.02 wide) and profile curvature (bins 0.001 wide) derived for different topography resolutions and the two study catchments.

bin j. The information content of the slope was computed by using bins 0.02 wide. The information content of profile curvature was computed by using bins 0.001 wide. The cumulative values of p_j are shown in Figure 10 for each DEM of the two study catchments, and the corresponding information contents are shown in Figure 11a. As expected, spatial aggregation resulted in a loss of information of slope gradient and curvature distribution. Figure 11a shows that when the grid size increases by 1 order of magnitude for the two catchments, the information content of slope decreases slightly, and the information content of profile curvature decreases greatly. These results are consistent with those of *Kuo et al.* [1999], who examined the effect of different grid sizes on information content of landscape representation data for a watershed in central New York.

[28] The curvature of the land surface is related to the second derivatives of the elevation data, which are multiplied by the soil hydraulic conductivity in the subsurface flow equation. In steep basins in particular, where topography is the main source of heterogeneity, these derivatives are the dominant factors of the equation. Thus hydraulic conductivity must partially compensate for the loss of information content of curvature distribution caused by spatial aggregation. In other words, the smoothed topography at larger grid sizes reduces the hydraulic gradient, which means the hydraulic conductivity must increase in order to produce the same rate of flow. To improve the macroscale hydrological simulation, the resulting information loss must be compensated for by an effective value of soil hydraulic conductivity K_S, which becomes larger than the small-scale value K_S^*.

[29] The loss of the landscape curvature information content due to spatial aggregation is thus related to the corresponding increase in the optimized values of hydraulic conductivity. A plot of the information content I of curvature distribution versus conductivity amplification factor α, combining the values reported in Figures 11a and 8a for each grid size, is shown in Figure 11b. There is very high correlation in both the basins ($r^2 = 0.99$) with the regression equation:

$$I = I^* - \ln \alpha, \tag{14}$$

where I^* is the information content of landscape curvature when the effective conductivity K_S tends to the value K_S^* derived from soil texture ($\alpha = 1$). The values $I^* = 7.8$ for basin 1 and $I^* = 8.8$ for basin 2 were obtained from the regression curves shown in Figure 11b. Values of $I < I^*$, between 6 and 8, could be obtained for the 1 m scale by correlating the information content with the grid size shown in Figure 11a. These values correspond to a conductivity amplification factor α between 3 and 5, i.e., $K_S > K_S^*$. Factors other than the smoothing of topography considered in this study could explain this difference. One example is macropores, whose effects on conductivity amplification may not be captured in a point measurement but are evident at larger scales. To apply equation (14) to other similar catchments the value of I^* may be evaluated using the

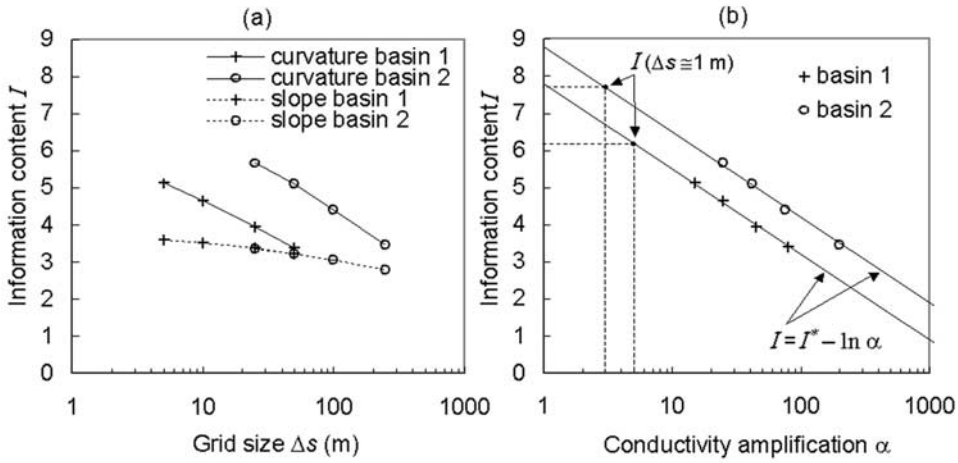

Figure 11. (a) Information content of slope and curvature distribution versus grid size; (b) information content of profile curvature versus optimized values of the hydraulic conductivity amplification factor for the two study catchments.

information content of small-scale terrain curvature (1 m scale), but also considering the other uncertainty factors, if a calibration equation for conductivity scaling is not available.

[30] By combining equations (11) and (14), and letting $\Delta I = (I^* - I) = ln\ \alpha$, the following relationship is derived:

$$K_S = K_S^*\ e^{\Delta I}. \tag{15}$$

Equation (15) can be used, for the basins tested, to provide an a priori estimate of the effective values at the grid scale of the hydraulic conductivity K_S, from the value K_S^* derived from soil texture, and from a grid analysis of the topographic characteristics of the landscape. For other similar basins, where the terrain curvature is also scale-dependent, equation (15) may be helpful in constructing a nested-grid model application. In this equation $\Delta I = (I^* - I)$ is the loss of information content between the point-scale complete information I^* (entropy = 0), and the grid scale reduced information I (entropy > 0). Thus ΔI is the Shannon entropy, which measures our ignorance of landscape topography and other hydrologic information at the grid scale [*Singh*, 1997]. Entropy of terrain curvature, as a measure of the loss of information content at different scales of spatial aggregation, may therefore be useful for correcting conductivity values when upscaling the subsurface flow equation in macroscale hydrological modeling. However, the approximations of the routing components and the simple conceptual representation of the water balance could lead to an overestimation of the space-scale effect on the hydraulic conductivity. Model applications with less approximations for the same or other catchments where saturation excess runoff prevails could resolve this, and future research will address this matter.

9. Conclusions

[31] Numerical methods for solving mathematical models of watershed hydrology involve the use of a discrete description of watershed geometry and parameters on a space-grid system. A crucial point is the degree of grid resolution used to describe the 3-D nature of terrain, and how model parameters are influenced by this. In this work, a parsimonious hydrology simulation was applied to two forested catchments with shallow and sloping soils, one medium and one small-sized, where saturation excess runoff prevails. Continuous simulation was used to examine the accuracy of the numerical schemes when solving the partial differential conservation equations of surface and subsurface flow routing in terms of the space-grid scale. The aggregation of the DEM as consequence of a coarse grid produced loss of information on watershed geometry and smoothed topographic relief. As a result the rate of flow was reduced as can be seen from sensitivity analysis of computed discharge. Calibration showed that the reduction of the second derivatives of the elevation data in the subsurface flow equation with spatial aggregation, may be compensated for by larger hydraulic conductivity values, especially when topography is the main source of heterogeneity.

[32] The informational concept of entropy was used to quantify the scale effect on parameter evaluation due to the spatial aggregation of topographic data. The loss of information content on terrain curvature distribution as grid size increases was related to the amplification factor required for the soil hydraulic conductivity, to compensate for the resulting retardation of the runoff hydrograph. A very high correlation was found for the hydrologic simulation of the two tested watersheds which links small-scale parameters with those required at the typically much coarser modeling scale. The derived equation can be used for the basins tested to estimate the effective value of hydraulic conductivity at the grid scale from the value derived from soil texture, using the information content of terrain curvature distribution derived from grid DEM. Similar results from two basin scales (4.5 and 123 km^2) and three flood runoff scales (0.5, 20, and 100 m^3/s) suggest that this technique could be a valid index of parameter rescaling. This technique may be helpful in constructing nested-grid model applications for other similar basins where the terrain curvature is also scale-dependent. Although the work deals with approximated flow routing components and a simple conceptual represen-

tation of the water balance, it could contribute to an understanding of the scale parameterization problem in numerical routing. Entropy of watershed curvature, as a measure of the loss of information content at different space scales, may be useful when upscaling the subsurface flow equation in macroscale hydrological modeling. When spatial aggregation is applied, the surface is smoother, entropy is higher, energy is reduced and upscaled hydraulic conductivity must be larger than point-scale measured values.

[33] The dissipation analysis of the numerical scheme used for this model showed that accuracy in the simulation of the detailed flow process within a storm event increases by using small space steps. As can be seen from the simulation tests, when spatial discretization of the 2-D subsurface flow routing scheme is small, the extent of the stream network along valley bottoms is more defined. The model, based on the "saturation excess" mechanism of runoff production, produces longer flow paths and longer travel time of surface flow, thus the channel response is more damped. The accuracy of the simulation could be verified by field measurements of the extent of saturated source areas. As space and time resolution have to be consistent with the accuracy and stability requirements of the numerical schemes, the hydrological processes should be represented at a scale which is smaller than the scale of the usually available climatic, topographic and soil data.

[34] **Acknowledgments.** The author wishes to thank the anonymous reviewers and the Associate Editor for their useful comments, suggestions and inputs. This research was funded by COFIN.

References

Abbott, M. B. (1992), *Computational Hydraulics*, Ashgate, Brookfield, Vt.

Abbott, M. B., J. C. Bathurst, J. A. Cunge, P. E. O'Connell, and J. Rasmussen (1986), An introduction to the European Hydrological System—Systeme Hydrologique Europeen "SHE," *J. Hydrol.*, *87*, 45–77.

Allen, R. G., L. S. Pereira, D. Raes, and M. Smith (1998), Crop evapotranspiration—Guidelines for computing crop water requirements, *FAO Irrig. Drain.*, 56.

Anderson, M. G., and T. P. Burt (1977), A laboratory model to investigate the soil moisture conditions on a drainage slope, *J. Hydrol.*, *33*, 383–390.

Bathurst, J. C., and P. E. O'Connel (1992), Future of distributed modeling: The Systeme Hydrologique Europeen, in *Terrain Analysis and Distributed Modeling in Hydrology*, edited by K. J. Beven and I. D. Moore, pp. 213–225, John Wiley, Hoboken, N. J.

Bergstrom, S., and L. P. Graham (1998), On the scale problem in hydrological modelling, *J. Hydrol.*, *211*, 253–265.

Beven, K. (1984), Infiltration into a class of vertically non-uniform soils, *J. Hydrol. Sci.*, *29*, 425–434.

Beven, K. (1989), Changing ideas in hydrology—The case of physically-based models, *J. Hydrol.*, *105*, 157–172.

Beven, K. (1995), Linking parameters across scales: Subgrid parameterizations and scale dependent hydrological models, *Hydrol. Processes*, *9*, 507–525.

Beven, K. J., R. Lamb, P. Quinn, R. Romanowicz, and R. Freer (1995), TOPMODEL, in *Computer Models of Watershed Hydrology*, edited by V. P. Singh, pp. 627–668, Water Resour. Publ., Highlands Ranch, Colo.

Bloschl, G., and M. Sivapalan (1995), Scale issues in hydrological modelling: A review, *Hydrol. Processes*, *9*, 251–290.

Bruneau, P., C. Gascuel-Odoux, P. Robin, P. Merot, and K. Beven (1995), Sensitivity to space and time resolution of a hydrological model using digital elevation data, *Hydrol. Processes*, *9*, 69–81.

Dickinson, R. E., A. Henderson-Sellers, C. Rosenzweig, and P. J. Sellers (1991), Evapotranspiration models with canopy resistance for use in climate models, a review, *Agric. For. Meteorol.*, *54*, 373–388.

Dingman, S. L. (1994), *Physical Hydrology*, 646 pp., Macmillan, Old Tappan, N. J.

Dunne, T., and R. D. Black (1970), An experimental investigation of runoff production in permeable soils, *Water Resour. Res.*, *6*, 478–490.

Finnerty, B. D., M. B. Smith, D.-J. Seo, V. Koren, and G. E. Moglen (1997), Space-time sensitivity of the Sacramento model to radar-gage precipitation inputs, *J. Hydrol.*, *203*, 21–38.

Fread, D. L. (1993), Flow routing, in *Handbook of Hydrology*, edited by D. R. Maidment, chap. 10, McGraw-Hill, New York.

Grayson, R. B., and G. Bloschl (2000), Spatial modelling of catchment dynamics, in *Spatial Patterns in Catchment Hydrology*, edited by R. B. Grayson and G. Bloschl, pp. 51–81, Cambridge Univ. Press, New York.

Grayson, R. B., I. D. Moore, and T. A. McMahon (1992a), Physically based hydrologic modeling: 1. A terrain-based model for investigative purposes, *Water Resour. Res.*, *28*, 2639–2658.

Grayson, R. B., I. D. Moore, and T. A. McMahon (1992b), Physically based hydrologic modeling: 2. Is the concept realistic?, *Water Resour. Res.*, *28*, 2659–2665.

Jensen, K. H., and A. Mantoglu (1992), Future of distributed modelling, in *Terrain Analysis and Distributed Modeling in Hydrology*, edited by K. J. Beven and I. D. Moore, pp. 203–212, John Wiley, Hoboken, N. J.

Kavvas, M. L. (1999), On the coarse-graining of hydrologic processes with increasing scales, *J. Hydrol.*, *217*, 191–202.

Koren, V. I., B. D. Finnerty, J. C. Schaake, M. B. Smith, D.-J. Seo, and Q.-Y. Duan (1999), Scale dependencies of hydrologic models to spatial variability of precipitation, *J. Hydrol.*, *217*, 285–302.

Kuo, W.-L., T. S. Steenhuis, C. E. McCulloch, C. L. Mohler, D. A. Weinstein, S. D. DeGloria, and D. P. Swaney (1999), Effect of grid size on runoff and soil moisture for a variable-source-area hydrology model, *Water Resour. Res.*, *35*, 3419–3428.

Legates, D. R., and G. J. McCabe (1999), Evaluating the use of "goodness-of-fit" measures in hydrologic and hydroclimatic model validation, *Water Resour. Res.*, *35*, 233–241.

Mendicino, G., and A. Sole (1997), The information content theory for the estimation of the topographic index distribution used in TOPMODEL, *Hydrol. Processes*, *11*, 1099–1114.

Moore, I. D., and R. B. Grayson (1991), Terrain-based catchment partitioning and runoff prediction using vector elevation data, *Water Resour. Res.*, *27*, 1177–1191.

Mosley, M. P. (1979), Streamflow generation in a forested watershed, New Zealand, *Water Resour. Res.*, *15*, 795–806.

Nash, J. E., and J. E. Sutcliffe (1970), River flow forecasting through conceptual models, part I—A discussion of principles, *J. Hydrol.*, *10*, 282–290.

Niedda, M. (1996), Use of network algorithms in spatially distributed models for the study of river basin response, in *Application of GIS in Hydrology and Water Resources Management*, edited by K. Kovar and H. P. Nachtnebel, *IAHS Publ.*, *235*, 207–214.

Niedda, M. (2000), Simulation of ground-water flow in steep basin with shallow surface soil, *J. Hydraul. Eng.*, *126*, 670–678.

Niedda, M., and G. Sechi (1996), A mixed optimization technique for large-scale water resource systems, *J. Water Resour. Plann. Manage.*, *122*, 1–10.

Paniconi, C., and E. F. Wood (1993), A detailed model for simulation of catchment scale subsurface hydrologic processes, *Water Resour. Res.*, *29*, 1601–1620.

Pearce, A. J. (1990), Streamflow generation processes: An austral view, *Water Resour. Res.*, *26*, 3037–3047.

Rawls, W. J., L. R. Ahuja, D. L. Brakensiek, and A. Shirmohammadi (1993), Infiltration and soil water movement, in *Handbook of Hydrology*, edited by D. R. Maidment, chap. 5, McGraw-Hill, New York.

Refsgaard, J. C. (1997), Parameterisation, calibration and validation of distributed hydrological models, *J. Hydrol.*, *198*, 69–97.

Refsgaard, J. C., M. Thorsen, J. B. Jensen, S. Kleeschulte, and S. Hansen (1999), Large scale modelling of groundwater contamination from nitrate leaching, *J. Hydrol.*, *221*, 117–140.

Rosso, R. (1994), An introduction to spatially distributed modelling of basin response, in *Advances in Distributed Hydrology*, edited by R. Rosso et al., pp. 3–30, Water Resour. Publ., Highlands Ranch, Colo.

Saulnier, G. M., K. Beven, and C. Obled (1997), Digital elevation analysis for distributed hydrological modelling: Reducing scale dependence in effective hydraulic conductivity values, *Water Resour. Res.*, *33*, 2097–2101.

Singh, V. P. (1997), The use of entropy in hydrology and water resources, *Hydrol. Processes*, *11*, 587–626.

Singh, V. P., and D. A. Woolhiser (2002), Mathematical modeling of watershed hydrology, *J. Hydrol. Eng.*, *7*, 270–292, doi:10.1061/(ASCE)1084-0699(2002)7:4(270).

Valeo, C., and S. Moin (2000), Grid-resolution effects on a model for integrating urban and rural areas, *Hydrol. Processes*, *14*, 2505–2525.

Vàzquez, R. F., L. Feyen, J. Feyen, and J. C. Refsgaard (2002), Effect of grid size on effective parameters and model performance of the MIKE-SHE code, *Hydrol. Processes*, *16*, 355–372, doi:10.1002/hyp.334.

Vieux, B. E. (1993), Aggregation and smoothing effects on surface runoff modeling, *J. Comput. Civ. Eng.*, *7*, 310–338.

Weiyan, T. (1992), *Shallow Water Hydrodynamics*, 474 pp., Elsevier Sci., New York.

Wigmosta, M. S., L. W. Vail, and D. P. Lettenmaier (1994), A distributed hydrology-vegetation model for complex terrain, *Water Resour. Res.*, *30*, 1665–1679.

Winchell, M., H. V. Gupta, and S. Sorooshian (1998), On the simulation of infiltration- and saturation-excess runoff using radar-based rainfall estimates: Effects of algorithm uncertainty and pixel aggregation, *Water Resour. Res.*, *34*, 2655–2670.

Wolock, D. M., and G. J. McCabe (2000), Differences in topographic characteristics computed from 100 and 1000 m resolution digital elevation model data, *Hydrol. Processes*, *14*, 987–1002.

Wood, E. F., M. Sivapalan, K. J. Beven, and L. Band (1988), Effects of spatial variability and scale with implications to hydrologic modelling, *J. Hydrol.*, *102*, 29–47.

Woods, R., M. Sivapalan, and M. Duncan (1995), Investigating the representative elementary area concept: An approach based on field data, *Hydrol. Processes*, *9*, 291–312.

Zhang, W., and D. R. Montgomery (1994), Digital elevation model grid size, landscape representation, and hydrological simulations, *Water Resour. Res.*, *30*, 1019–1028.

M. Niedda, Dipartimento di Ingegneria del Territorio, Universita di Sassari, Via De Nicola, I-07100 Sassari, Italy. (niedda@ssmain.uniss.it)